Ultra-High Density Arrays of Defect Free AlN Nanorods: A 'Space Filling' Approach

Michele Conroy[†‡§‖], *Vitaly Z. Zubialevich*[†], *Haoning Li*[†‡], *Nikolay Petkov*[†], *Sally O'Donoghue*[†§], *Justin D. Holmes*[†§‖], *Peter J. Parbrook*[*†‡]

[†] Tyndall National Institute, Dyke Parade, Cork City, Ireland

[‡] School of Engineering, University College Cork, Cork City, Ireland

[§] Department of Chemistry, University College Cork, Cork City, Ireland

[‖] AMBER@CRANN, Trinity College Dublin, Dublin City, Ireland

KEYWORDS: III-nitrides, nanowires, nanorods, aluminum nitride, growth mechanism

ABSTRACT

Nanostructured semiconductors have a clear potential for improved optoelectronic devices, such as high efficiency light emitting diodes (LEDs). However most arrays of semiconductor nanorods suffer from having relatively low densities (or "fill factors") and a high degree of non-uniformity, especially when produced by self-organized growth. Ideally an array of nanorods for an optoelectronic emitter should have a fill factor close to 100 %, with uniform rod diameter and height. In this article we present for the first time, a new 'space-filling' approach for forming

defect-free arrays of AlN nanorods, whereby the separation between each rod can be controlled to 5 nm due to a self-limiting process. These arrays of pyramidal topped AlN nanorods formed over wafer-scale areas by metal organic chemical vapour deposition (MOCVD), provide a defect free semi-polar top surface, for potential optoelectronic device applications with the highest reported fill factor at 98%.

III-N materials are commonly nanostructured, to filter out unwanted dislocations.[1-4] The high lattice mismatch, at 12 % for example between sapphire and AlN, leads to high threading dislocation densities (TDD).[5] The large surface-to-volume ratio of a nanowire compared to bulk III-N, allows for very efficient lattice relaxation and hence defect free materials to be created.[6-8] In optoelectronics, the ability to fully control crystal quality and dimensions of an active region is necessary for the realization of highly efficient photonic devices.[9,10] Another major advantage of using nanorods as the template for solid state lighting is the possibility to explore active region epitaxial growth on preferred planes such as semi-polar and non-polar facets. These newly exposed planes allow growth, of quantum wells that do not suffer from the severe band distortion caused, by piezoelectric fields that is an issue with c-plane polar (0001) orientated growth.[11,12]

Nanorod arrays with high fill factors also lead to a much more efficient usage of substrate compared to planar growth. Close packed nanorods have the potential to counter act the well-known issue of droop in III-Ns by reduced current densities in the junction at constant total currents.[13] There have been major steps achieved in recent years in the controllable growth of III-N nanowires, specifically GaN.[14,15] Most recently, single photon emission at room temperature has been demonstrated on GaN/AlGaN nanorods made by selective area growth,[16] and for AlN dramatic improvements in the emission of a deep ultraviolet light emitting diode, and in

particular in its electrical properties has been reported through the application of a nanorod approach.[17] However the fundamental problem with growing desirable highly dense arrays of III-N nanorods is their tendency to coalesce forming continuous layers.[18,19] The initial radial growth of nanorods is known to begin immediately after nucleation,[20] resulting in coalescence early on if the density of the rods is very high in growth both by MOCVD and molecular beam epitaxy. Along with radial growth, out-of-plane misorientation of III-N nanorods has been investigated in depth, especially for GaN.[21,22] Mutual misorientation is not only one cause of coalescence in III-N layers, it also results in inhomogeneous strain during heteroepitaxial thin film growth.[18,23] The resulting defects at grain boundaries between newly coalesced nanorods form non-recombination centres, detrimental to the crystal perfection and future applications of arrays of nanorods.[24,25] The problem of growing ultra-high density non-coalesced arrays of III-N nanorods, although investigated in depth, has not been answered to date. In this article we present the first synthesis of wafer-scale, dislocation-free arrays of AlN nanorods via an MOCVD space filling approach. The ultra-dense arrays have stable gaps of 5 nm, which is the smallest value reported for any semiconductor material based nanorods as far as we know. As a result we have produced arrays of nanorods with a fill factor up to 98%.

RESULTS AND DISCUSSION

Ultra-high density AlN nanorods were formed by patterning planar AlN films using a nanosphere lithography (NSL) approach, as illustrated in Figure 1a(i), originally designed for epitaxial lateral overgrowth coalesced layers of AlN.[1] However, for this study an extended inductively coupled (ICP) etch time was used to “over-etch” the AlN causing a tapered profile to the etched rods, as seen in Figure1 b, due to mask reshaping. After removal of the residual silica sphere hard mask (SSHM) by a buffered oxide etch (BOE) in step (ii) of Figure 1a, AlN was

grown on the etched seed nanorod templates by MOCVD, producing the rods in step (iii) of Figure 1a schematic. Figure 1c shows scanning electron microscope (SEM) top-down and tilted scans of perfectly hexagonal 6-sided topped AlN rods (mean height = 3μm, mean diameter = 330nm and mean nanorod spacing = 5 nm), grown after 100 min in the reactor. Extending the growth time to 200 min AlN nanorods with an identical surface geometry (in terms of diameter nanorod spacing), but a mean height of 7 μm were achieved, as shown in Figure 1d. All nanorods produced had sharp tips, independent of growth time. These structures could be readily exfoliated as individual nanorods from the substrate to prove they were free standing and absent of coalescing despite the narrow gaps between them. From the SEM images shown in Figure 1, the grown rods expand both laterally and vertically from the etched template features, but eventually lateral growth is quenched leaving a space of 5nm, which remains constant with increasing rod length. This self-limited lateral expansion between adjacent rods stops the coalescence process normally observed in GaN growth.[18] The geometry of the 6 sided apex tipped nanorods is similar to that reported for GaN rods obtained by selective area growth.[27] The nanorod array on the wafer scale takes on the form of a 2-dimensional poly-crystal, consistent with the self-organised nature of the nanosphere mask. The hexagonal rods show some shape deformation at the grain boundaries between ordered regions of spheres, as shown by way of example within the Supporting Information of Figure S3. Similar effects are observed where a nanosphere void occurred. No evidence of rod coalescence was found associated with the self-organised nature of the mask used.

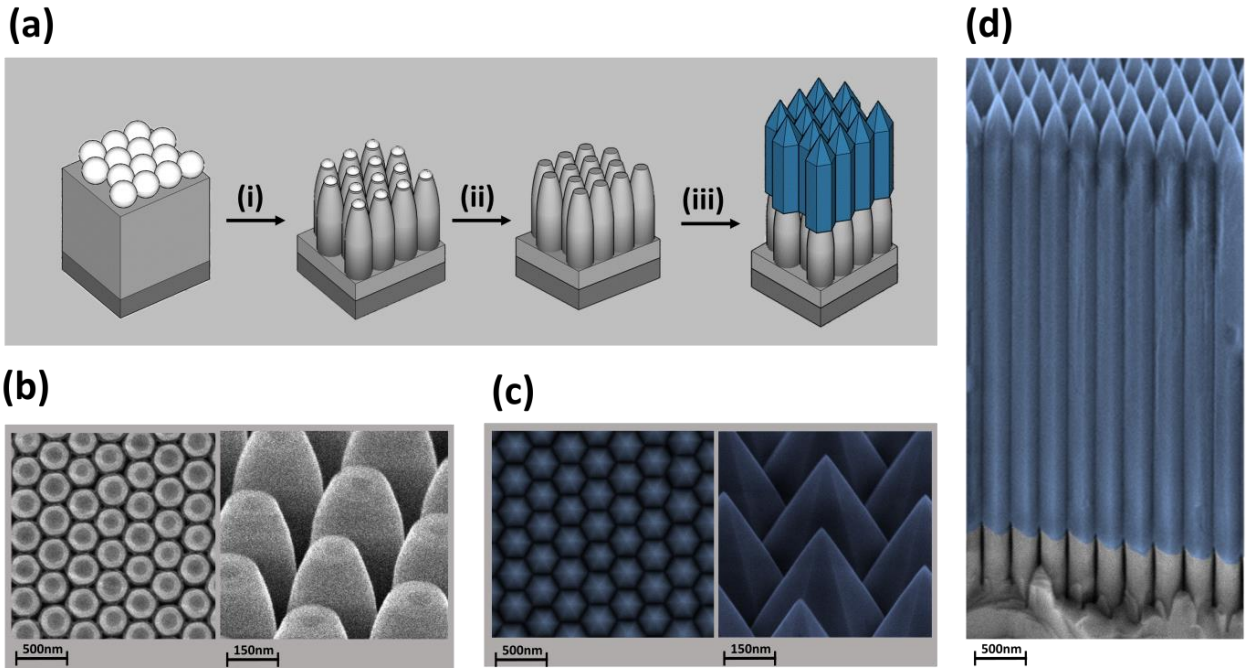

Figure 1. Experimental method to grow space filling AlN nanorods investigated by a SEM study of the surface morphology. (a) Schematic of the dry ICP etching of the SSHM producing nanorods in step (i), followed by the removal of the SSHM with BOE before MOCVD AlN growth in step (iii), (b) SEM images of the original nano-patterned template, (c) SEM images of the resulting growth on top of the template shown in (b), and (d) SEM cross section of nanorods formed by doubling the growth time of (c).

In order to confirm the wurzite non-polar and semi-polar facet orientations of the AlN nanorods, rows of the nanorods were cross-sectioned by Focused Ion Beam (FIB) in the 10-10 direction for transmission electron microscopy (TEM) analysis, as seen in Figure 2a. The non-polar side walls were determined to be (1-100) facets, whilst the "slanted" rod tops, at an angle of 62°, correspond to semi-polar (1-101) facets, as reported in literature,[28] see Figures 2c and f. High resolution imaging of the area between each rod confirmed an air gap of 5 nm, Figures 2c,d and in the Supporting Information Figure S3.5. The nanorods were scratched off the template onto a

poly-carbon TEM grid, Figure 2e, to investigate the sharp tip unaffected by FIB damage as seen in the cross sectional tips Figure 2f. No dislocations were visible in the nanorods under bright field TEM imaging, see Figures 2a and b. After the TEM samples were tilted in the g = 11-20 and g = 0002 under the 2 beam weak beam dark field (WBDF) conditions neither edge, screw or mixed type dislocations were visible. These WBDF images confirmed the dislocation free nature of the AlN nanorods grown by MOCVD. A detailed bright field and WBDF TEM investigation, seen in Figure 2h and the Supporting Information Figure S3.1, of the original etched rod template below the overgrown layer illustrates the dislocation filtering by lattice relaxation of the high aspect ratio of the etched nanorods. The majority of the dislocations bend into the surrounding airgaps before over-growth during the pre-growth annealing process, as reported previously.[26]

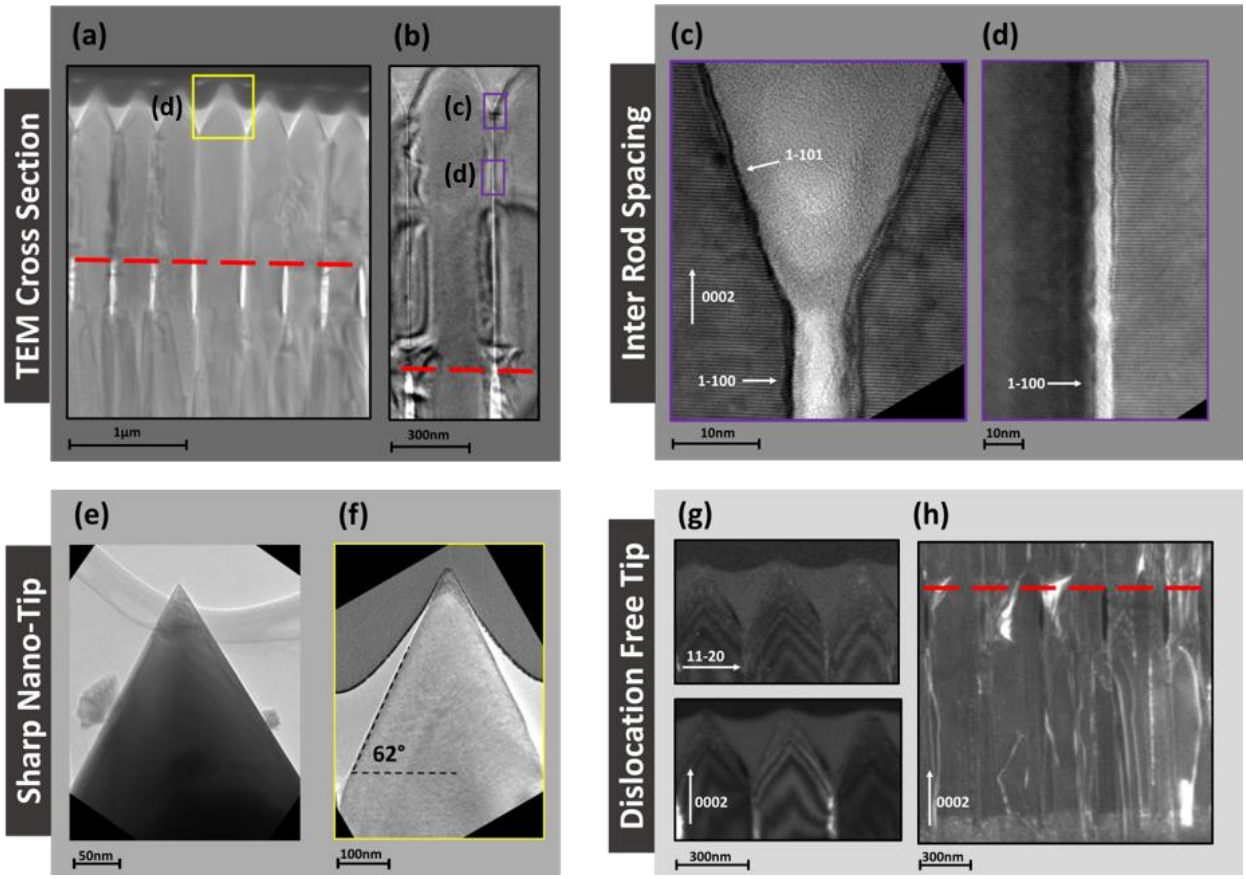

Figure 2. Experimental results obtained by TEM to confirm the 5nm air gap and dislocation free nature of the nanorods. TEM Cross Section: (a) bright field image of the AlN nanorods, (b) higher magnification of a revealing the gaps between nanorods. Inter Rod Spacing: (c) lattice resolution image of area in (b) where the semi-polar facets of two nanorods meet, (d) lattice resolution image of area in (b) of the inter-rod spacing. Sharp Nano Tip: (e) sharp tip of a nanorod scratched off onto a TEM poly-carbon grid unaffected by FIB damage, (f) higher resolution image of nano-tip area in a revealing the 62° semi-polar facet top. Dislocation Free Tip: (g) Weak Beam Dark Field (WBDF) images of the top of the rods tilted in g = (11-20) and g = (0002).

Having confirmed experimentally the possibility of growing compound semiconductor ultra-dense space filling nanorods, we investigated the effect of original pattern geometry on the subsequent AlN nanorod growth. We first deposited a monolayer of larger 700 nm silica spheres and spaced these features out using a CF_4 dry ICP etch to shrink the nanospheres as in Figure 3 a (I). Following this two "over-etched" nanorod templates were formed; pattern (II) was etched for 1 min giving an etch depth of 450 nm with rod top diameter of 300 nm and pattern (III) was etched for 2 min giving an etched depth of 900 nm and rod top diameter of 100 nm. AlN grown on top of these two strikingly different geometries of etched nanorods resulted in identical semi-polar (1-101) apex tipped nanorods as shown in Figure 3b. From TEM analysis of the inter-nanorod spacing of these two resulting nanorod arrays shown in the Supporting Information Figure S3.4 the spacing again stayed constant at 5 nm. Thus the space filling arrays of rods are remarkably stable with changing template geometry under the growth conditions used.

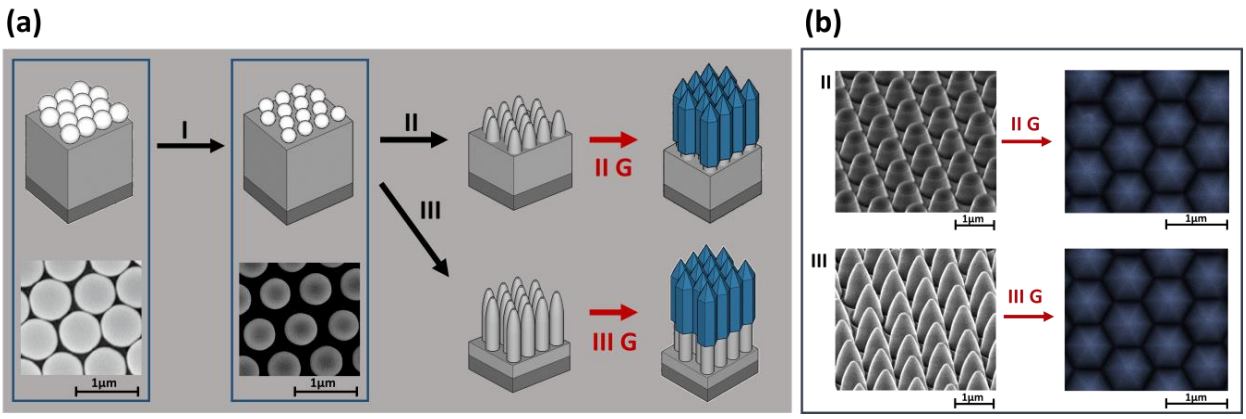

Figure 3. Experimental verification of the space filling growth mode of AlN grown on spaced out etched rods. (a) Illustration of the etching steps forming AlN spaced out nanorod patterns and subsequent growth, with SEM image insets of the silica spheres before and after the oxide ICP etch in step I, (b) SEM images of step II after the 1min Cl2 ICP etch, step III after the 2min Cl_2 ICP etch, and after steps IIG and IIIG where AlN was grown on top of the over-etched rods.

To investigate the development of the rod profile, a series of growth thickness experiments were performed on the over-etched nanorod pattern. Figure 4 reveals how the facets develop before space filling occurs. At the very early stage of growth, formation of the 1-101 semi-polar plane facets, area between solid and dashed circles, reveal themselves as the slowest growing plane. As growth continues, the area occupied by the 1-101 facets increases (Figures 4 b to d, marked with a dashed circle). Initially, vertical growth of nanorods is significantly suppressed (Figures 4f-h), most likely due to a strong consumption of Al adatoms in forming the 1-101 facets, until their height is comparable or less than the 1-101-plane Al adatom diffusion length. Later, not all Al-adatoms can reach the bottom 1-101 plane border and they start to contribute more towards vertical growth (Figure 4i). Meanwhile, the 1-101-planes continue to expand downwards until

they first meet their nonpolar m-planes (Figure 4d) and, finally, until they occupy all available space, *i.e.* until semi-polar planes of adjacent are nearly touching each other (Figure 4e).

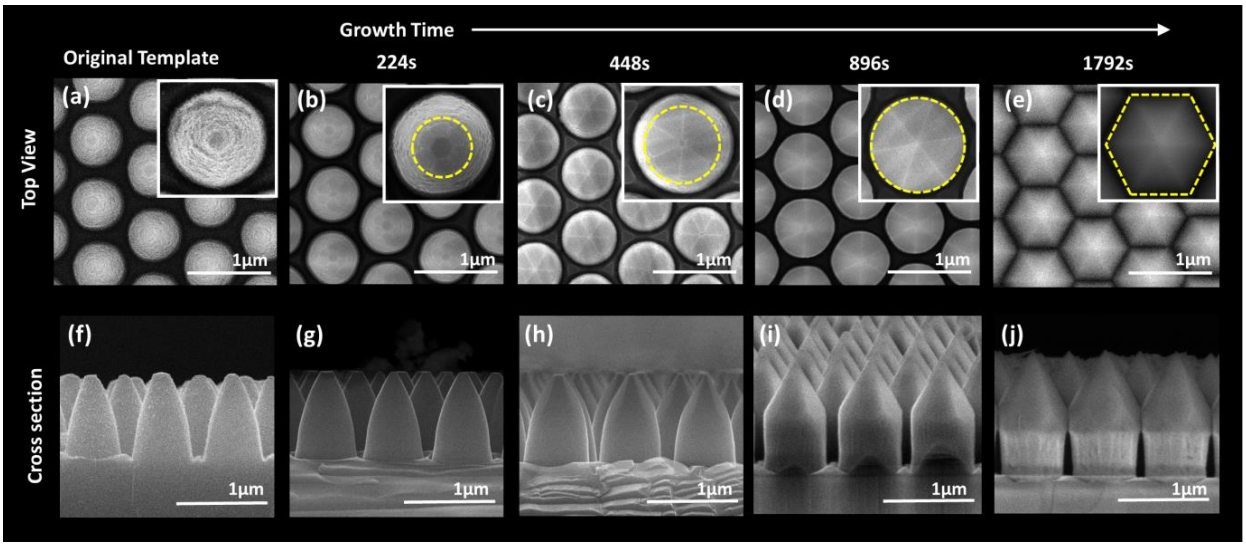

Figure 4. Formation of 10-11 semi-polar side facets obtained by SEM of the AlN nanorod growth thickness series. SEM top down images of: (a) AlN over-etched nanorod template with remaining top c-plane surface, (b)-(e) growth thickness series of AlN deposited on template (a) showing with increased growth time the c-plane diameter decreases and the semi-polar facets grow out to fill the space between the rods (yellow dashed line), SEM cross sectional images of: (f) AlN over-etched nanorod template, (g)-(j) increasing growth time of AlN growth thickness series of AlN deposited on template (f) showing with increased growth time the c-plane diameter decreases and the semi-polar facets grow out to fill the space between the rods, additionally the vertical height increases only after the c-plane diameter approaches zero.

The growth mechanism for the evolution in shape of the grown AlN nanorods will be broken into two parts; (i) the formation of the initial apex tipped surface morphology and (ii) vertical growth

without coalescence as in Figure 5a. We put forward a mechanism to describe the two possible outcomes of growth at stage (i); case 1/rod formation as reported here and case 2/coalesced bulk layer formation[26]. Our observation is if the c-plane is too small(relative to the rod diameter), as seen in Figure 4, or even missing, then the competition between the c-plane and the 1-101-facets of the nanorods will become and/or continue to grow apex-topped. This dominant c-plane vertical growth for case 1 is illustrated in Figure 5b. If contrarily the c-plane facet is relatively large compared to the potential semi-polar plane, *i.e.* a small gap between the c-plane facets of adjacent rods/vertical rod sidewalls, then the c-plane will further expand until the semi-polar planes disappear in case 2. This leads to nanorod coalescence forming a smooth flat layer as reported elsewhere[26] and illustrated in Figure 5b. The schematics shown in Figures 5b represent the case of a shrinking or increasing c-plane (following the red dashed line) by examining the influence of the slowest growing facet. To back up this growth mechanism, we have formulated a mathematical model of nanorod growth, taking into account the solid angles at which facets accept adatoms from the ambient environment, the diffusion lengths of Al-adatoms on different facets and the probabilities of adatom migration between facets, schematically represented in Figure 5c and detailed in the Supporting Information Figure S4.2. While the model is too complex to have an analytical solution and many assumptions for unknown quantities are an issue, the model does show that in the two limits of relative c-plane and semi-polar plane areas that either nanorod growth or coalescence will be preferred, as we observe experimentally, Supporting Information Figure S4.1.

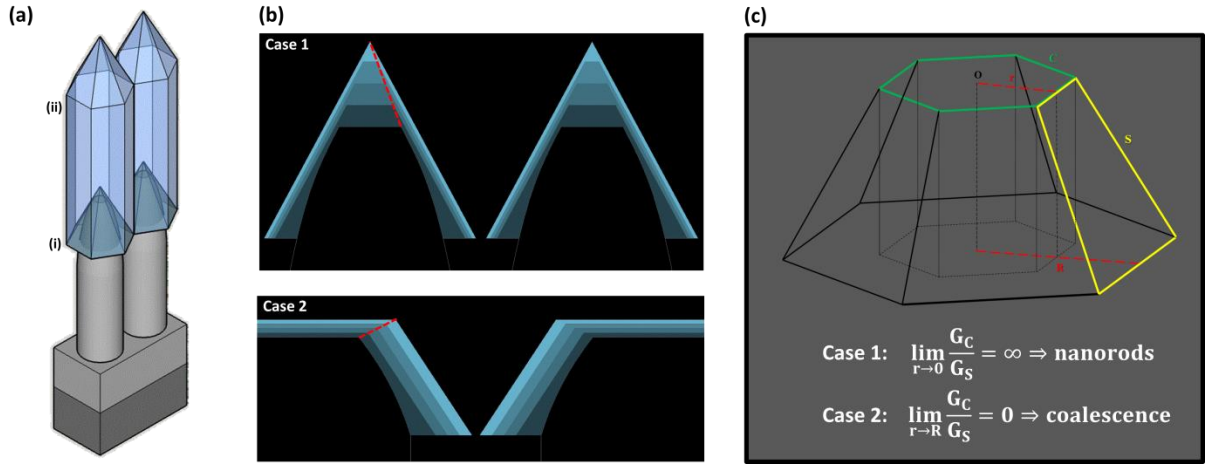

Figure 5. Illustration of the growth mechanism for the formation of the initial surface morphology of the AlN nanorod growth. (a) 3D representation of the two steps in the growth mechanism (i) the formation of the initial apex tipped surface morphology and (ii) vertical growth without coalescing , (b) case 1 schematic showing the evolving growth thickness with a higher vertical growth rate, dashed line showing the shrinking of the c-plane facet, (c) case 2 where the growth rate in the semi-polar direction is higher, dashed line showing the expansion of the c-plane facet, (d) skeleton drawing of the surface geometry at step (i), illustrating the main parameters of the growth model and the resulting growth equations.

Figure 5 c shows the main parameters analysed in the mathematical model to calculate the resulting growth surface profile. As described in Figure 5c for case 1, when the top c-plane radius (r) approaches zero the limit of the ratio of the c-plane growth rate (G_c) over the semi-polar growth rate (G_S) equals infinity and results in nanorod formation. However for case 2, when the top c-plane radius (r) approaches the rod radius (R) the limit of the ratio of the c-plane growth rate (G_c) over the semi-polar growth rate (G_s) equals zero and hence the semi-polar facets disappear completely allowing coalescence of the rods. One can understand this qualitatively by

considering the Al-adatom exchange between competing c- and semi-polar facets. Being small, a facet adsorbs a proportionally small amount of adatoms from the ambient and therefore it is kinetically unfavorable to supply a material to its adjacent facets, thus giving only a small contribution to the adjacent facet growth rate. On the other hand, the facet being small by receiving even a small fraction of adatoms from its much larger adjacent facet can grow relatively quickly. In such a way the smaller facet growth rate is higher and thus that facet will shrink further and eventually disappear.

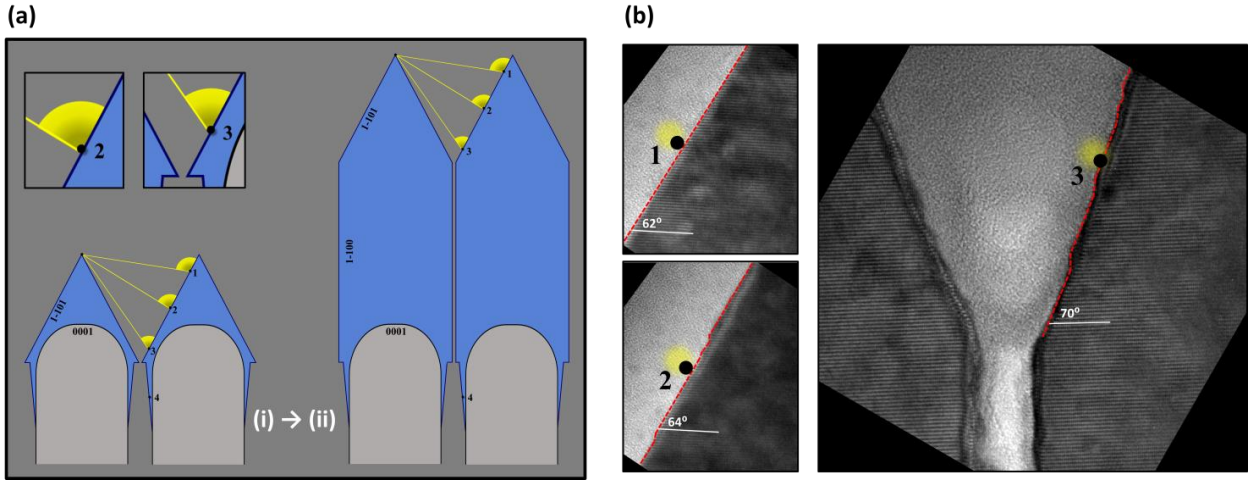

Figure 6. Progressively steeper facets of the semi-polar sidewall with increased flux shielding by neighboring rod resulting in self-limited lateral growth. (a) Schematic drawing of the formation of the (1-100) sidewalls after increased growth time (deposition thickness) on (i), showing the decreased incoming flux Φ from points 1→3, (b) TEM images at points 1, 2 and 3 revealing progressively steeper facet formation (red dashed lines) on the (1-101) sidewall with decreasing incoming flux, and in turn increasing (1-101) sidewall angle to the (0001) growth plane.

The second stage (ii) of the growth mechanism, is the remarkable evolution of vertically growing space filling without coalescence, illustrated schematically in Figure 5a(ii) and Figure 6a(ii). To describe the reasoning behind the rods' stabilising against coalescence, we combined our growth model from step (i) with that reported by Falub *et al.*[29] for germanium micro-pillars (MPs) grown on silicon MPs. As described in their report, they detail a macro model for the evolution of the top of their pillars based on a reduced surface diffusion and non-uniformity in the incoming flux Φ with growth thickness. However they do not resolve the microscopic mechanism that determines the 50 nm spacing between their MPs. Nonetheless, they do put forward the idea that the quenching of lateral growth is most probably due to flux shielding of the incoming gaseous reactants when the spacing between their towers shrinks below tens of nanometers.

In case 1 of our AlN nanorods the negligible growth on the m-plane (1-100) side walls of the over-etched rods, as seen by SEM in Figure 4g→j, leads us to believe that the incoming flux angle is near zero due to nearest nanorod shielding. As seen earlier by SEM imaging in Figure 4e and j, when the semi-polar facets are completely formed they spread out to fill the space forming a canopy over the non-polar sidewall fully shielding any incoming flux, represented by the magnified point 3 of Figure 6a. The schematic drawing of the change in flux shielding Figure 6a reveals the decreased incoming flux angle down the semi-polar (1-101) sidewall (points 1→3). With decreasing incoming flux angle (points 1→3) there is progressively steeper facet formation on the semi-polar sidewall, as seen in high resolution TEM of Figure 6b. Any incoming Al adatoms reaching the steep the steep (~70°) facet stepped semi-polar sidewall near point 3, are used up in trying to form the preferred smooth (1-101) facet angle of 62° as found higher up the sidewall (point 1). In our case 2 the absence of the semi-polar facet effectively eliminates the extreme flux shielding effect found in case 1, causing the rods to coalesce. Thus the feature

determining the rod development is the formation of significant semi-polar (1-101) facets prior to the rods nearly touching to allow apex tops to stabilize which consequently leads to rod stabilization due to flux shielding.

Conclusion

The results presented above provide the long awaited answer to growing ultra-dense arrays of III-N nanorods at wafer scale. The stable gaps between rods of 5 nm results in the highest reported space filling factor of 98%, as well as being the first report of a space filling growth mode seen in compound semiconductors. This apex tops produced potentially provide a semi-polar faceted dislocation free template on which quantum wells could be prepared, which both have larger surface area than a planar layer and much reduced polarization fields, both of which effects should reduce the instantaneous carrier density in an LED under operation and hence substantially reduce efficiency droop effects. The rod formation process can be controlled simply by altering the initial etching of an AlN template layer, allowing us to change the resulting growth from a coalesced bulk AlN layer to arrays of nanorods. The growth mode is determined to be governed by the original template geometry rather than by the growth parameters. An additional advantage of this method to form arrays of nanorods is that it can be formed by a simple self-assembly patterning technique, avoiding the need for additional expensive lithography processing steps. Finally, the nanorods produced showed high structural quality with no evidence of dislocations or stacking faults propagating to the top surface.

Methods

Nanosphere Lithography

The spheres were synthesised by the Stöber[30] method in ethanol to a diameter of 330 ±5 nm, 550 ±5 nm, and 700 ±10 nm. Before patterning a solution was made up of the silica spheres in ethanol at 10% w/v and chloroform at a ratio of 2:3 and stirred for 30 min. This mixture was then introduced to the surface of a trough of water by a glass dropper with an AlN/sapphire wafer already submerged as previously described by Oh et al.[31] The glass trough was then lowered mechanically allowing the self-assembly of the silica particles on the emerging wafer piece, photograph in Supporting Information Figure S1. A chlorine based inductively coupled plasma ICP dry etch (etch recipe details can be found in the supporting information) was used to transfer the pattern into the underlying AlN film forming the structures using Oxford Instruments Plasmalab 100 model. The remaining silica mask after etching was removed by soaking the film in a bath of buffered oxide solution (Sigma Aldrich ammonium fluoride – hydrofluoric acid mixture) for 5 mins to ensure a silica free surface before placing the film back in the reactor. To space out the silica sphere pattern before using the AlN etch a CF_4 based etch was used as described in S1.

Growth of AlN nanorods by MOCVD

The initial AlN film was grown on c-plane sapphire substrates ($0.10° \pm 0.02°$ miscut towards the m-plane) using an Aixtron close coupled showerhead 3 x 2" MOCVD reactor. As presented in our previous work[32] a three step temperature variation recipe was used to grow the films to a thickness of 2µm in the MOCVD reactor. After these AlN films were patterned by NSL they

were placed back into the reactor for further growth. The MOCVD growth conditions for the re-deposition of AlN used were as follows: 1100^0C growth temperature, V/III ratio 50 and pressure 100 mbar. In-situ reflectance measurements were carried out using a Laytec EpiTT system to record the growth, as seen in supporting information Figure S2. The susceptor surface temperature was measured by a pyrometer and compared to the spot measurements using an ARGUS CCS Pyrometric Profiling System multi-channel pyrometer for more accurate representation of the surface temperature variation during growth.

Structural Characterisations

SEM was utilized to obtain a visual representation of the overgrowth surface and as a method to understand the behavior of the in situ reflectivity measurements, using a FEI Quanta 650 field emission gun (FEG) high resolution SEM. The crystal structure and defect analysis was characterised on all samples using a JEOL 2100 200 kV high resolution transmission electron microscope (TEM). Cross sectional TEM specimens were prepared with a focused ion beam (FIB) using a FEI HELIOS NanoLab 600 dual-beam system. The type and density of the TDs were investigated by weak beam dark field TEM imaging. For detailed analysis of the dislocation movement within the crystal structure the sample was cut in the (10-10) and (11-20) zone axes. The samples were then tilted to a 2 beam condition in the g = (11-20) and g = (10-10) directions respectively, where only the edge and mixed (edge and screw) type dislocations were visible. Screw TDD was determined by tilting the samples in the (0002) direction.

AUTHOR INFORMATION

Corresponding Author

* Address correspondence to peter.parbrok@tyndall.ie

Present Addresses

†‡§‖Michele Conroy: Pacific Northwest National Laboratory, 902 Battelle Blvd, Richland, WA 99354, United States.

Author Contributions

The manuscript was written through contributions of all authors. All authors have given approval to the final version of the manuscript.

Conflict of Interest: The authors declare no competing financial interest.

S*upporting Information Available:* Detailed sample preparation of the self-assembled etch hard mask, MOCVD in-situ reflectance monitoring, TEM dislocation movement study, detailed mathematical model of the proposed growth mechanism. This material is available free of charge via the Internet at http:// pubs.acs.org.

Acknowledgment. This research was enabled by the Irish Higher Education Authority Programme for Research in Third Level Institutions Cycles 4 and 5 via the INSPIRE and TYFFANI projects, and by Science Foundation Ireland (SFI) under Grant no. SFI/10/IN.1/I2993. PJP acknowledges funding from SFI Engineering Professorship scheme (07/EN/E001A) and MC acknowledges PhD research scholarship from INSPIRE. This work was conducted under the framework of the Irish Government's Programme for Research in Third Level Institutions Cycle 5, National Development Plan 2007–2013 with the assistance of the European Regional

Development Fund. We also acknowledge the support of Dr Mahbub Ahkter for his support with fabrication and William Jagoe for his illustrations in the article.

REFERENCES

1. Colby, R.; Liang, Z.; Wildeson, I. H.; Ewoldt, D. A.; Sands, T. D.; García, R. E.; Stach, E. A., Dislocation Filtering in GaN Nanostructures. Nano Letters **2010**, 10 (5), 1568-1573.

2. Nabarro, F. R. N., Mathematical theory of stationary dislocations. Advances in Physics **1952**, 1 (3), 269-394.

3. Nabarro, F. R., Theory of crystal dislocations. **1967**.

4. Eshelby, J. D., Screw Dislocations in Thin Rods. Journal of Applied Physics **1953**, 24 (2), 176-179.

5. Shetty, S.; Ghatak, J.; Shivaprasad, S. M., Surface nitridation induced AlN nano-columnar growth on c-sapphire. Solid State Communications **2014**, 180, 7-10.

6. Avit, G.; Lekhal, K.; André, Y.; Bougerol, C.; Réveret, F.; Leymarie, J.; Gil, E.; Monier, G.; Castelluci, D.; Trassoudaine, A., Ultralong and Defect-Free GaN Nanowires Grown by the HVPE Process. Nano Letters **2014**, 14 (2), 559-562.

7. Li, S. F.; Fuendling, S.; Wang, X.; Merzsch, S.; Al-Suleiman, M. A. M.; Wei, J. D.; Wehmann, H. H.; Waag, A.; Bergbauer, W.; Strassburg, M., Polarity and Its Influence on

Growth Mechanism during MOVPE Growth of GaN Sub-micrometer Rods. Crystal Growth & Design **2011**, 11 (5), 1573-1577.

8. Songmuang, R.; Katsaros, G.; Monroy, E.; Spathis, P.; Bougerol, C.; Mongillo, M.; De Franceschi, S., Quantum Transport in GaN/AlN Double-Barrier Heterostructure Nanowires. Nano Letters **2010**, 10 (9), 3545-3550.

9. Yan, R.; Gargas, D.; Yang, P., Nanowire photonics. Nat Photon **2009**, 3 (10), 569-576.

10. Reithmaier, J. P., Nanostructured Semiconductor Materials for Optoelectronic Applications. In Nanostructured Materials for Advanced Technological Applications, Reithmaier, J.; Petkov, P.; Kulisch, W.; Popov, C., Eds. Springer Netherlands: **2009**, 447-476.

11. Yeh, T.-W.; Lin, Y.-T.; Stewart, L. S.; Dapkus, P. D.; Sarkissian, R.; O'Brien, J. D.; Ahn, B.; Nutt, S. R., InGaN/GaN multiple quantum wells grown on nonpolar facets of vertical GaN nanorod arrays. Nano Letters **2012**, 12 (6), 3257-3262.

12. Ra, Y.-H.; Navamathavan, R.; Kang, S.; Lee, C.-R., Different characteristics of InGaN/GaN multiple quantum well heterostructures grown on m- and r-planes of a single n-GaN nanowire using metalorganic chemical vapor deposition. Journal of Materials Chemistry C **2014**, 2 (15), 2692-2701.

13. Waag, A.; Wang, X.; Fündling, S.; Ledig, J.; Erenburg, M.; Neumann, R.; Al Suleiman, M.; Merzsch, S.; Wei, J.; Li, S.; Wehmann, H. H.; Bergbauer, W.; Straßburg, M.; Trampert, A.; Jahn, U.; Riechert, H., The nanorod approach: GaN NanoLEDs for solid state lighting. physica status solidi (c) **2011**, 8 (7-8), 2296-2301.

14. Chesin, J.; Zhou, X.; Gradečak, S. In Light extraction in individual GaN nanowires on Si for LEDs, **2012,** 846703-10.

15. Hsu, Y.-C.; Sou, K.-P.; Chang, S.-P.; Hsu, K.-S.; Shih, M. H.; Kuo, H.-C.; Cheng, Y.-J.; Chang, C.-Y., Room temperature ultraviolet GaN metal-coated nanorod laser. Applied Physics Letters **2013**, 103 (19).

16. Holmes, M. J.; Choi, K.; Kako, S.; Arita, M.; Arakawa, Y., Room-Temperature Triggered Single Photon Emission from a III-Nitride Site-Controlled Nanowire Quantum Dot. Nano Letters **2014**, 14 (2), 982-986.

17. Zhao, S.; Connie, A. T.; Dastjerdi, M. H. T.; Kong, X. H.; Wang, Q.; Djavid, M.; Sadaf, S.; Liu, X. D.; Shih, I.; Guo, H.; Mi, Z., Aluminum nitride nanowire light emitting diodes: Breaking the fundamental bottleneck of deep ultraviolet light sources. Scientific Reports. **2015**, 5, 8332.

18. Brandt, O.; Fernández-Garrido, S.; Zettler, J. K.; Luna, E.; Jahn, U.; Chèze, C.; Kaganer, V. M., Statistical Analysis of the Shape of One-Dimensional Nanostructures: Determining the Coalescence Degree of Spontaneously Formed GaN Nanowires. Crystal Growth & Design **2014**, 14 (5), 2246-2253.

19. Dong, P.; Yan, J.; Wang, J.; Zhang, Y.; Geng, C.; Wei, T.; Cong, P.; Zhang, Y.; Zeng, J.; Tian, Y.; Sun, L.; Yan, Q.; Li, J.; Fan, S.; Qin, Z., 282-nm AlGaN-based deep ultraviolet light-emitting diodes with improved performance on nano-patterned sapphire substrates. Applied Physics Letters **2013**, 102 (24).

20. Fernández-Garrido, S.; Kaganer, V. M.; Sabelfeld, K. K.; Gotschke, T.; Grandal, J.; Calleja, E.; Geelhaar, L.; Brandt, O., Self-regulated radius of spontaneously formed GaN nanowires in molecular beam epitaxy. Nano Letters **2013**, 13 (7), 3274-3280.

21. Jenichen, B.; Brandt, O.; Pfueller, C.; Dogan, P.; Knelangen, M.; Trampert, A., Macro- and micro-strain in GaN nanowires on Si (111). Nanotechnology **2011**, 22 (29), 295714.

22. Wierzbicka, A.; Zytkiewicz, Z.; Kret, S.; Borysiuk, J.; Dluzewski, P.; Sobanska, M.; Klosek, K.; Reszka, A.; Tchutchulashvili, G.; Cabaj, A., Influence of substrate nitridation temperature on epitaxial alignment of GaN nanowires to Si (111) substrate. Nanotechnology **2013**, 24 (3), 035703.

23. Kaganer, V.; Jenichen, B.; Brandt, O.; Fernández-Garrido, S.; Dogan, P.; Geelhaar, L.; Riechert, H., Inhomogeneous strain in GaN nanowires determined from x-ray diffraction peak profiles. Physical Review B **2012**, 86 (11), 115325.

24. Park, C.; Park, Y.; Im, H.; Kang, T., Optical properties of GaN nanorods grown by molecular-beam epitaxy; dependence on growth time. Nanotechnology **2006**, 17 (4), 952.

25. Consonni, V.; Knelangen, M.; Jahn, U.; Trampert, A.; Geelhaar, L.; Riechert, H., Effects of nanowire coalescence on their structural and optical properties on a local scale. Applied Physics Letters **2009**, 95 (24), 241910.

26. Conroy, M.; Zubialevich, V. Z.; Li, H.; Petkov, N.; Holmes, J. D.; Parbrook, P. J., Epitaxial lateral overgrowth of AlN on self-assembled patterned nanorods. Journal of Materials Chemistry C **2015**, 3 (2), 431-437.

27. Nakajima, K.; Ujihara, T.; Miyashita, S.; Sazaki, G., Effects of misfit dislocations and AlN buffer layer on the GaInN/GaN phase diagram of the growth mode. Journal of Applied Physics **2001**, 89 (1), 146-153.

28. Wang, G. T.; Li, Q.; Wierer, J. J.; Koleske, D. D.; Figiel, J. J., Top–down fabrication and characterization of axial and radial III-nitride nanowire LEDs. Physica Status Solidi (a) **2014**, 211, (4) 748-751.

29. Falub, C. V.; von Känel, H.; Isa, F.; Bergamaschini, R.; Marzegalli, A.; Chrastina, D.; Isella, G.; Müller, E.; Niedermann, P.; Miglio, L., Scaling Hetero-Epitaxy from Layers to Three-Dimensional Crystals. Science **2012**, 335 (6074), 1330-1334.

30. Stöber, W.; Fink, A.; Bohn, E., Controlled growth of monodisperse silica spheres in the micron size range. Journal of colloid and interface science **1968**, 26 (1), 62-69.

31. Oh, J. R.; Moon, J. H.; Yoon, S.; Park, C. R.; Do, Y. R., Fabrication of wafer-scale polystyrene photonic crystal multilayers via the layer-by-layer scooping transfer technique. Journal of Materials Chemistry **2011**, 21 (37), 14167-14172.

32. Li, H.; Sadler, T. C.; Parbrook, P. J., AlN heteroepitaxy on sapphire by metalorganic vapour phase epitaxy using low temperature nucleation layers. Journal of Crystal Growth **2013**, 383 (0), 72-78.